Inorganic Films from Three Different Phosphors via a Liquid Coating Route from Inverse Miniemulsions

Andreas Taden,[†] Markus Antonietti,[†] Anne Heilig,[†] and Katharina Landfester*[,‡]

Max Planck Institute of Colloids and Interfaces, Research Campus Golm, 14424 Potsdam, Germany, and Organic Chemistry III Macromolecular Chemistry, University of Ulm, Albert-Einstein-Allee 11, 89081 Ulm, Germany

Received January 6, 2004. Revised Manuscript Received July 30, 2004

Precursor nanoparticles of complex lanthanide phosphors with binary and ternary composition are made using the inverse miniemulsion process. These particles show a high colloidal and compositional stability and are used to obtain inorganic crystalline films which can be very thin and highly homogeneous in topography and structure. In a subsequent annealing process, the precursor materials are converted to films of red, green, or blue phosphor. In the case of red phosphor, "single-crystal films" are formed which show a surface roughness of the order of single crystalline surfaces.

Introduction

The application of polymer films from their aqueous dispersions is a convenient and environmentally friendly approach to high-performance coatings. In the application, the dispersion consisting of polymer particles in water is transformed into a void-free and mechanically continuous polymer film which, after film formation, is no longer sensitive to water.[1] In this process, the particles must be deformed into space-filling polyhedra which can occur if the application temperature exceeds the so-called minimum film-forming temperature of the system.

Due to the usually high melting points of inorganic nanoparticles, a simple liquid-dispersion-based film formation is not reported in the literature, and even sintering at elevated temperatures mostly leads to monolithic, but porous materials. This is why continuous inorganic films are still mostly applied via other methods; e.g., chemical vapor deposition (CVD)-type approaches using volatile precursors,[2] electrodeposition from solution,[3] ion beam sputter deposition,[4] or pulsed laser deposition.[5]

Finely dispersed metal salts and nanoparticles, on the other hand, are widely used in numerous technological and medical applications; e.g., as ceramic precursors, filler materials, pigments, recording materials, in electronics, catalysis, medical diagnostics, and many others. Several techniques have been developed for the generation of such particles, some based on physical principles, some based on chemical principles. With mechanical grinding or so-called colloidal milling, particles smaller than 1 μm are not accessible, the grain distribution is broad, and the shape is irregular due to the nondirected cracking. This is why wet-chemical procedures are of larger importance, since they allow, in principle, control of size and shape. Besides standard precipitation or controlled nucleation-and-growth processes (such as the Stöber process[6]), which take place from homogeneous starting solutions, reactions in biphasic media such as microemulsions[7] or miniemulsions have moved into the focal zone of interest,[8] since they are convenient and very save, plus they offer an additional synthetic parameter by the length scale and structure of the primary biphasic system.

In this paper we will use the inverse miniemulsion process to obtain well-defined inorganic particles in an organic solvent which diminishes corrosion and allows convenient further processing of the particles. Miniemulsions are understood as liquid/liquid emulsions consisting of small, long-time stable, and narrowly size-distributed droplets with diameters between 30 and 300 nm. The process of miniemulsion can be best described by applying extreme shear forces to a system consisting of a continuous phase, a dispersed phase, a surfactant, and an osmotic pressure agent which prevents the droplets from Ostwald ripening. In the reported inverse miniemulsions,[9] a liquid hydrophilic monomer was emulsified in a hydrophobic phase such as cyclohexane or other hydrocarbons by using high shear. The inverse miniemulsion obtains its stability by using a combina-

* To whom correspondence should be addressed. E-mail: katharina.landfester@chemie.uni-ulm.de.
[†] Max Planck Institute of Colloids and Interfaces.
[‡] University of Ulm.

(1) Winnik, M. A. In *Emulsion Polymerization and Emulsion Polymers*; El-Aasser, M. S., Lovell, P. A., Eds.; Wiley: Chichester, 1997; pp 468−517.
(2) Pierson, H. O. *Handbook of Chemical Vapor Deposition Principles, Technology and Applications*; Noyes Data Corporation/Noyes Publications: Norwich, NY, 1999.
(3) Dini, J. W.; Dini, J. W. *Electrodeposition: The Materials Science of Coatings and Substrates*; Materials Science and Process Technology Series; Noyes Data Corporation/Noyes Publications: Norwich, NY, 1993.
(4) Hemment, P. L. F. *Ion Beam Processing of Materials and Deposition Processes of Protective Coatings*; Progress in Biotechnology; Elsevier Science: Amsterdam, 1996.
(5) Chrisey, D. B., Hubler, G. K., Eds. *Pulsed Laser Deposition of Thin Films*; Wiley-Interscience: New York, 1996.
(6) Stöber, W.; A., F.; Bohn, E. *J. Colloid Interface Sci.* **1968**, *1*, 62.
(7) Pileni, M. P. *Adv. Colloid Interface Sci.* **1993**, *46*, 139−163.
(8) Antonietti, M.; Landfester, K. *Prog. Polym. Sci.* **2002**, *27*, 689−757.
(9) Landfester, K.; Willert, M.; Antonietti, M. *Macromolecules* **2000**, *33*, 2370−2376.

10.1021/cm049958+ CCC: $27.50
Published on Web 11/03/2004

tion of an effective surfactant and an osmotic pressure agent which is practically insoluble in the continuous phase and prevents the minidroplets from Ostwald ripening. In the case of inverse miniemulsions, this is ideally an ionic salt. During the following conversions (e.g., polymerization or polyaddition), it was shown that each droplet can be considered as an independent nanoreactor, and ideally, the droplets convert in a one-to-one copy process under preservation of particle number and the amount and relative composition of material in each droplet.

The technique of miniemulsion was already transferred to liquids with still higher cohesion energy, namely high salt containing ionic liquids and liquid metals.[10] These miniemulsions can subsequently be further reacted to nanoparticles and nanostructures which can be high-melting and insoluble.

In this contribution we will make use of the high colloidal and composition stability of miniemulsion droplets to synthesize well-defined precursor nanoparticles of complex lanthanide phosphors with binary and ternary compositions. In addition, we will show that it is possible to make continuous and very smooth inorganic films of some of these functional inorganic materials from the liquid state, based on appropriately composed inverse miniemulsions.

Experimental Section

Materials. Magnesium (II) nitrate pentahydrate (99%), aluminum (III) nitrate nonahydrate (98%), yttrium (III) nitrate hexahydrate (99.9%), europium (III) nitrate pentahydrate (99.9%), lanthanium (III) nitrate hexahydrate (99.99%), cerium (III) nitrate hexahydrate (99.99%), terbium (III) nitrate pentahydrate (99.9%), barium acetate (99%), nitric acid (70 wt % in water, ACS reagent), and phosphoric acid (85 wt % in water, ACS reagent) were all purchased from Aldrich and used as received. Cyclohexane was a gift from BASF and of technical grade. The block copolymer emulsifier poly(butylene-*co*-ethylene)-*b*-poly(ethylene oxide) (PB/E-PEO) consisting of a hydrophobic block ($M_w = 3700$ g·mol^{-1}) and a hydrophilic block ($M_w = 3600$ g·mol^{-1}) was synthesized starting from Kraton L (Shell) dissolved in toluene by adding ethylene oxide under the typical conditions of anionic polymerization.[11] Alternatively, Lubrizol U, a polyisobutylene succinimide (from Lubrizol Co.), was also applied as an inverse stabilizer.

Synthesis. *Red Phosphor 1.* To obtain red phosphor particles of $Y_{0.94}Eu_{0.06}(NO_3)_3$, 3.582 g (9.4 mmol) of $Y(NO_3)_3 \cdot 6\ H_2O$ and 0.257 g (0.6 mmol) of $Eu(NO_3)_3 \cdot 5\ H_2O$ were dissolved in 4.0 g of water. This aqueous solution was added to a solution consisting of 16.0 g of cyclohexane (boiling point at 80.7 °C) and 160 mg of the copolymer PB/E-PEO. After vigorously stirring for 1 h, the miniemulsion was prepared by ultrasonicating the emulsion for 2 min with a Branson sonifier W450 ($^1/_2$-in. tip) at 90% amplitude under ice cooling.

The water was removed by heating the miniemulsion to 60 °C for 8 h in an open vessel. Cyclohexane was added stepwise to avoid the complete drying of the sample.

Green Phosphor. To obtain green phosphor particles of $La_{0.5}Ce_{0.3}Tb_{0.2}PO_4$, 1.299 g (3.0 mmol) of $La(NO_3)_3 \cdot 6\ H_2O$, 0.782 g (1.8 mmol) of $Ce(NO_3)_3 \cdot 6\ H_2O$, and 0.522 g (1.2 mmol) of $Tb(NO_3)_3 \cdot 5\ H_2O$ were dissolved in 2.5 g of water and 1.5 g of concentrated nitric acid (70 wt % HNO_3 in water). Afterwards, 0.692 g of concentrated phosphoric acid (85 wt % H_3PO_4 in water) was added. Without nitric acid, precipitation is observed upon addition of the phosphoric acid.

This solution was added to a solution consisting of 16.0 g of cyclohexane and 160 mg of the copolymer PB/E-PEO. After vigorously stirring for 1 h, the miniemulsion was prepared by ultrasonicating the emulsion for 2 min with a Branson sonifier W450 ($^1/_2$-in. tip) at 90% amplitude under ice cooling.

The water was removed by heating the miniemulsion to 60 °C for 8 h in an open vessel. Cyclohexane was stepwise added to avoid the complete drying of the sample.

Blue Phosphor. Barium acetate (0.115 g, 0.45 mmol), 0.021 g of $Eu(NO_3)_3 \cdot 5\ H_2O$ (0.05 mmol), 0.128 g of $Mg(NO_3)_2 \cdot 5\ H_2O$ (0.5 mmol), and 1.876 g of $Al(NO_3)_3 \cdot 9\ H_2O$ (5.0 mmol) were dissolved in 6.0 g of water at a temperature of 60 °C and added to a solution with the same temperature of 180 mg of the copolymer PB/E-PEO in 18.0 g of cyclohexane. The mixture was vigorously stirred for 5 min, and afterwards the miniemulsion was prepared by ultrasonicating the emulsion for 3 min with a Branson sonifier W450 ($^1/_2$-in. tip) at 90% amplitude under slight cooling with a 20 °C water bath.

The water was removed by heating the miniemulsion to 60 °C for 8 h in an open vessel. Cyclohexane was added stepwise to avoid the complete drying of the sample.

Drying/Heating. The samples were dried at room temperature in a desiccator under reduced pressure (membrane pump vacuum).

The heating protocol was as follows.

At 200 °C. Heating to 100 °C within 1 h; constant temperature of 100 °C for 2 h; further heating to 200 °C within 1 h; constant temperature of 200 °C for 6 h (the samples were taken out of the oven after cooling to room temperature, and the cooling rate was not defined).

At 1000 °C. Heating to 200 °C within 1 h; constant temperature of 200 °C for 2 h; further heating to 1000 °C within 4 h; constant temperature of 1000 °C for 6 h (the samples were taken out of the oven after cooling to room temperature, and the cooling rate was not defined).

Methods. *Atomic Force Microscopy (AFM).* Atomic force microscopy was performed with a NanoScope IIIa microscope (Digital Instruments, Santa Barbara, CA) operating in tapping mode. The instrument was equipped with a 10 × 10 μm e-scanner and commercial silicon tips (model TSEP, the force constant was 50 N·m^{-1}, the resonance frequency was 300 kHz, and the tip radius was smaller than 20 nm). For the preparation of the monolayer film, the samples were diluted with cyclohexane to a solid content of ca. 8% and then spin-coated at a spinning speed of 4000 rpm for 30 s. The silicon substrate was previously cleaned by applying the standard RCA-I-process (heating the substrate to 80 °C for 10 min in a 5:1:1 mixture of water, 30 wt % H_2O_2, and 25 wt % NH_3) in order to remove organic contaminants.

Wide-Angle X-ray (WAXS). The wide-angle X-ray diffraction was measured in a Nonius CP120 Diffractometer using a Cu Kα radiation ($\lambda = 1.54$ Å).

Dynamic Light Scattering (DLS). The particle sizes were measured using a Nicomp particle sizer (model 370, PSS Santa Barbara, CA) at a fixed scattering angle of 90°.

Transmission Electron Microscopy (TEM). Electron microscopy was performed with a Zeiss 912 Omega electron microscope operating at 100 kV. The diluted colloidal solutions were applied to a 400-mesh carbon-coated copper grid and left to dry; no further contrasting was applied.

Karl Fischer Titration. The water contents were measured with a Metrohm Ionenanalytik 756 KF Coulometer using Hydranal-Coulomat AD (Riedel-de Haen) solutions.

Results and Discussion

The precursor nanoparticles and the homogeneous inorganic films are made from the substances red phosphor ($(Y_{0.94}Eu_{0.06})_2O_3$), green phosphor ($La_{0.5}Ce_{0.3}Tb_{0.2}PO_4$), and blue phosphor ($Ba_{0.90}Eu_{0.1}MgAl_{10}O_{17}$). The names already indicate the color of luminescence when these substances are excited by electron beams,

(10) Willert, M.; Rothe, R.; Landfester, K.; Antonietti, M. *Chem. Mater.* **2001**, *13*, 4681−4685.

(11) Schlaad, H.; Kukula, H.; Rudloff, J.; Below, I. *Macromolecules* **2001**, *34*, 4302−4304.

Table 1. Characteristics of the Different Precursor Miniemulsions[a]

sample	surfactant content [wt %] without water	surfactant content [wt %] including water	d_I [b] [nm]	Gaussian polydispersity[b] [%]	water content of droplets [wt %]
blue phosphor (BP)	8.4	2.2	154	27.2	44
red phosphor (RP)	4.2	2.0	207	11.0	48
green phosphor (GP)	3.8	2.2	223	33.7	43

[a] Cyclohexane was used as continuous phase and PB/E-PEG was used as nonionic surfactant. [b] Obtained from DLS.

as these are the three luminescent materials which are used in television screens. Red phosphor can be obtained from the precursor material $Y_{0.94}Eu_{0.06}(NO_3)$ after an annealing process at temperatures above 1000 °C. For achieving the stoichiometry, the correct ratio of $Y(NO_3)_2 \cdot 6\ H_2O$ and $Eu(NO_3)_2 \cdot 5\ H_2O$ was dissolved in water to form a ca. 50 wt % aqueous solution. This solution was transferred to miniemulsion droplets in an organic solvent as continuous phase. As nonionic surfactants, amphiphilic block copolymers are preferentially applied. Obviously, the salts themselves act as osmotic pressure agents since they are not soluble in the continuous phase, and therefore they prevent the droplets efficiently from Ostwald ripening.

Blue and green phosphor can be produced from annealing the corresponding precursor compounds at temperatures of 1000 °C or above. The synthesis of the precursor miniemulsions follows the same principle as presented in case of the red phosphor. In the case of blue phosphor $Eu(NO_3)_2 \cdot 5\ H_2O$, $Mg(NO_3)_2 \cdot 5\ H_2O$, $Al(NO_3)_3 \cdot 9\ H_2O$, and barium acetate are transferred to an aqueous solution, keeping the exact predefined stoichiometry. Instead of barium acetate, the nitrate salt of barium can be applied as well. Because of the lower water solubility of these salts, a relatively high amount of water and nonionic surfactant has to be used for the primary dispersion step.

The green phosphor precursor miniemulsion can be produced by dissolving the salts $La(NO_3)_2 \cdot 6\ H_2O$, $Ce(NO_3)_3 \cdot 6\ H_2O$, and $Tb(NO_3)_3 \cdot 5\ H_2O$ in a strong nitric acid environment, followed by the addition of phosphorous acid in the exact stoichiometry.

The three very different recipes just demonstrate the high chemical flexibility and stability of inverse miniemulsions, as prepared above. It must be stated that corresponding microemulsions would require much lower salt concentrations and would offer a much lower stability against chemical variations and pH changes.

For further application of the dispersion, such as film formation, where fast evaporation of the continuous phase is needed, a continuous phase with a low boiling point, e.g. cyclohexane, is favorable. However, stable dispersions can also be obtained for different organic solvents such as heptane (bp 98 °C), octane (bp 125 °C), and Isopar M (bp range between 199 and 257 °C). As nonionic surfactant PB/E-PEG or Lubrizol U were applied. In all cases, except for the combination of Lubrizol U/green phosphor (the surfactant is protonated by the strong acids), stable miniemulsions can be prepared. By determining the residue water content with Karl Fischer titration and the solid content of the resulting dispersions, the percentage of water inside the corresponding dispersion droplets can be calculated. The content of molecular dissolved water in the organic solvent (e.g., 0.0034 wt % for cyclohexane) was neglected. Furthermore, size and size distribution were characterized by DLS. The results for the corresponding dispersions with cyclohexane as continuous phase and PB/E-PEG as nonionic surfactant are summarized in Table 1.

The relative surfactant content without water is only referring to the solid content and is important for the film formation. The percentage of surfactant with water is referring to the whole dispersed phase and is of key importance for the stability of the miniemulsion and has a big influence on the droplets size and distribution. In any case, it is seen that the relative amount of stabilizer in the final film is comparably low.

It is also interesting to note that the water content of the droplets after evaporation of the water at 60 °C for several hours is still relatively high and is reaching a threshold value, typical for strongly bound water along ions and interfaces. In the case of blue phosphor, the applied nitrate salts possess a content of 40 wt % hydrate water, and the employed barium acetate is hydroscopic. For the applied red phosphor precursor salts, the hydrate water content is theoretically 28 wt %, but a higher water content of 48 wt % was calculated. For green phosphor, the hydrate water content of the used nitrate salts is 20 wt %, but the employed concentrated nitric and phosphoric acid are strongly hygroscopic. The remaining water content will turn out to be important for film formation.

The films were prepared as described in the experimental part from the precursor dispersions listed in Table 1 and were characterized with respect to film homogeneity and crystallinity. A comparative set of WAXS measurements has been made from the original liquid dispersions and from the dried but not calcined material and is shown in Figure 1. All measurements and the drying were performed at room temperature.

The green phosphor precursor has no crystallinity in either dispersion or in the dried state (see Figure 1a and b). The amorphous halo at about 20° scattering angles in the dispersion samples is due to the liquid structure of cyclohexane. Because of the strong hydroscopic acids necessary for the preparation of this sample, the formation of crystalline structures is obviously suppressed for this sample.

For the red phosphor precursor, the X-ray measurement shows no crystallinity of the dispersion, but there is a nicely organized crystalline structure in the thin film. This system definitely crystallizes throughout film formation.

In the case of the blue phosphor dispersion, already in the dispersion one can observe single and sharp peaks at 17.9°,41.3°, 48.0°, and 70.6°. Interestingly, these peaks cannot be found in the corresponding dried material, which is again highly crystalline. This is obviously due to a recrystallization toward a different

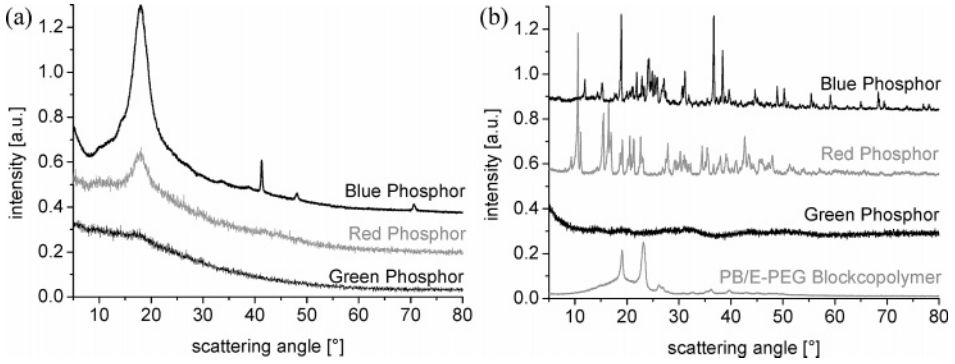

Figure 1. (a) WAXS diagrams from the precursor dispersions of blue, red, and green phosphors in cyclohexane. The blue phosphor sample shows sharp peaks which reflect high crystallinity. (b) WAXS diagrams of the utilized block copolymer and of the dispersions after drying at room temperature.

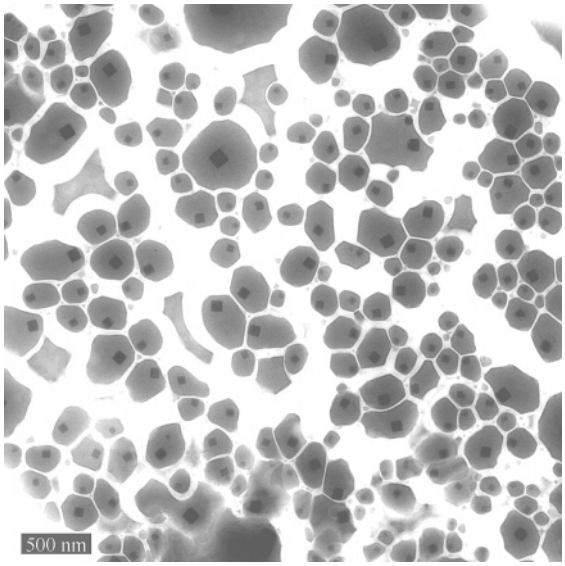

Figure 2. TEM micrograph of the blue phosphor precursor dispersion.

compound, as also indicated by the TEM of a submonolayer of such a dispersion after drying (Figure 2).

One can nicely see that the starting situation is essentially a liquid situation, with the stabilizer still keeping most of the droplets separated and only allowing partial coalescence. Complete film formation is prohibited by the submonolayer situation, which also makes heterogeneous nucleation rather ineffective.[12] Figure 2, however, shows that each droplet contains mostly one discrete single crystal with uniform cubic shape, while this crystal size is proportional to the size of the corresponding domain. This crystal most probably consists of barium nitrate, in agreement with the WAXS peaks of the original miniemulsion. The formed crystals stay trapped in the particles and cannot growth further, and the colloidal stability of the sample is obviously not affected by this crystal inclusion. This species is then later consumed while crystallizing also the other inorganic components of the droplets.

The green and red phosphor precursor droplets also can be characterized by TEM in submonolayer conditions. In good agreement with the amorphous character identified by WAXS, the green phosphor droplets seem to keep their spherical character and the particle number throughout the drying process (Figure 3a). The size and polydispersity of the spherical nanoparticles corresponds to the values of DLS, i.e., Figure 3a gives also a nice illustration of the quality of dispersion in the original inverse salt miniemulsion.

For the red phosphor sample after drying, rather well-defined polyhedral crystals of up to 500 × 200 nm are detected. It seems that in this case each nanodroplet re-crystallizes to a single crystal, taking up all different inorganic components in a single structure. As one can look through the crystals, they are rather thin platelets. Assuming preservation of particle number (i.e., one

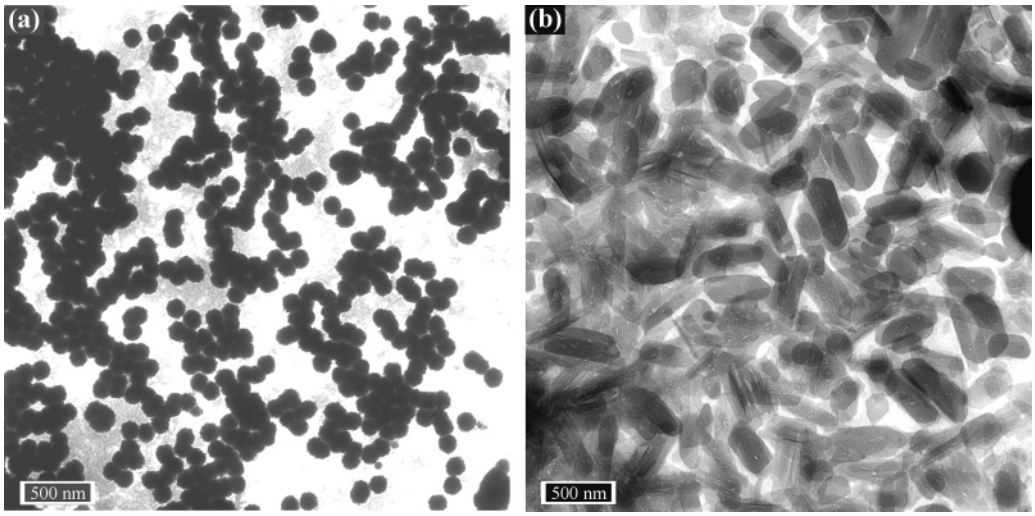

Figure 3. TEM micrographs of (a) green phosphor and (b) red phosphor after drying under submonolayer conditions.

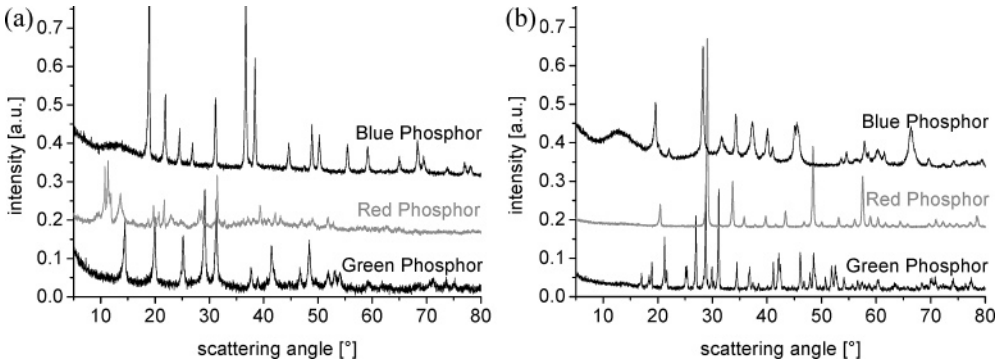

Figure 4. WAXS diagrams from the blue, red, and green phosphor samples after annealing at (a) 200 °C and (b) 1000 °C (see references; e.g., in refs 13 and 14).

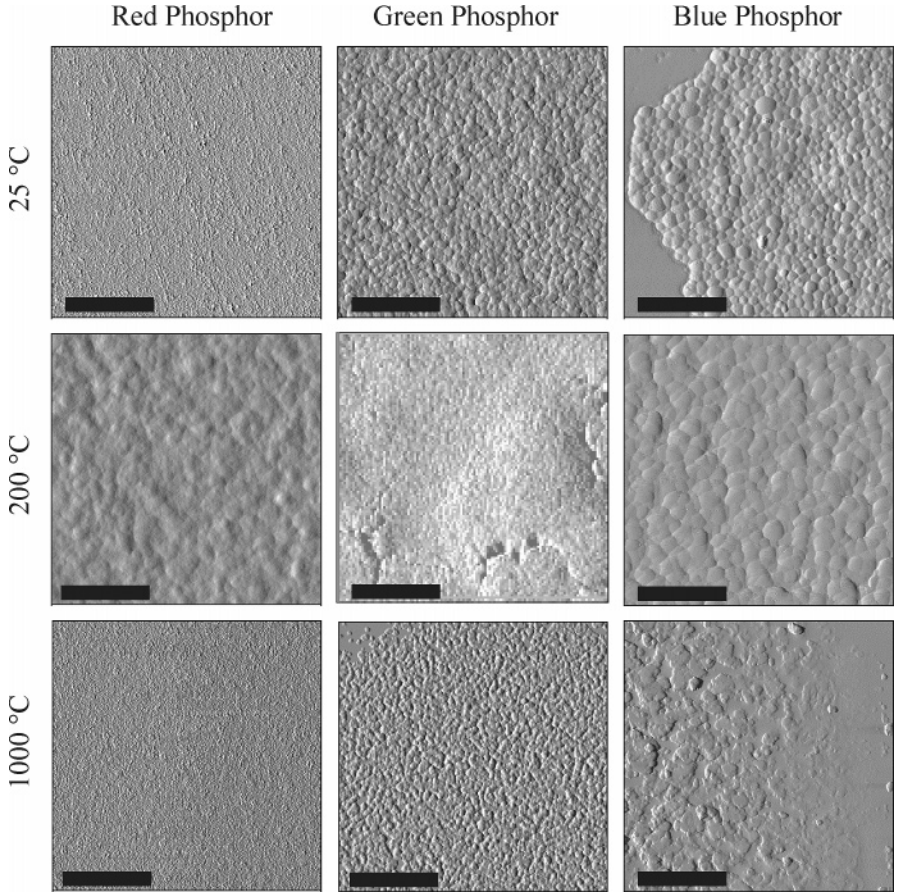

Figure 5. AFM amplitudes pictures of red, green, and blue phosphor films at room temperature and after annealing at 200 and 1000 °C. The bar corresponds to 1 μm.

nucleation center per droplet), constant particle volume before and after crystallization would give an estimate for the thickness of about 20 nm.

After having characterized the three dispersions with their very different characters (amorphous, solid/liquid, highly crystallizable), we want to examine the structure of their films in the functional state after calcination. It is the special charm of a liquid precursor to allow easy application and lateral structuration, such as spray and spin coating, or classical or ink jet printing.

Here, we analyzed the ability to create thin and homogeneous films by spin coating and subsequent calcination of the characterized precursor dispersions. A temperature of ca. 1000 °C is needed to transform the precursors into the corresponding oxide or phosphate "phosphor" material. For this purpose, a droplet of a precursor dispersion with a solid content of ca. 8 wt % was spread on a silicon wafer which acted as a model substrate. For the X-ray measurements, the dried precursor dispersion powders were annealed under the same conditions. For a better characterization of the transformation process, the annealing process was ramped at 200 and 1000 °C under air atmosphere, and the intermediates were also characterized.

The WAXS measurements (see Figure 4) confirm the successful solid-phase reaction of the precursors into the

(12) Montenegro, R.; Antonietti, M.; Mastai, Y.; Landfester, K. *J. Phys. Chem.* **2003**, *107*, 5088−5094.
(13) Kottaisamy, M.; Horikawa, K.; Kominami, H.; Aoki, T.; Azuma, N.; Nakanishi, Y.; Hatanaka, Y. *Bull. Electrochem.* **1999**, *15*, 312−314.
(14) Kim, K.-B.; Kim, Y.-I.; Chun, H.-G.; Cho, T.-Y.; Jung, J.-S.; Kang, J.-G. *Chem. Mater.* **2002**, *14*, 5045−5052.

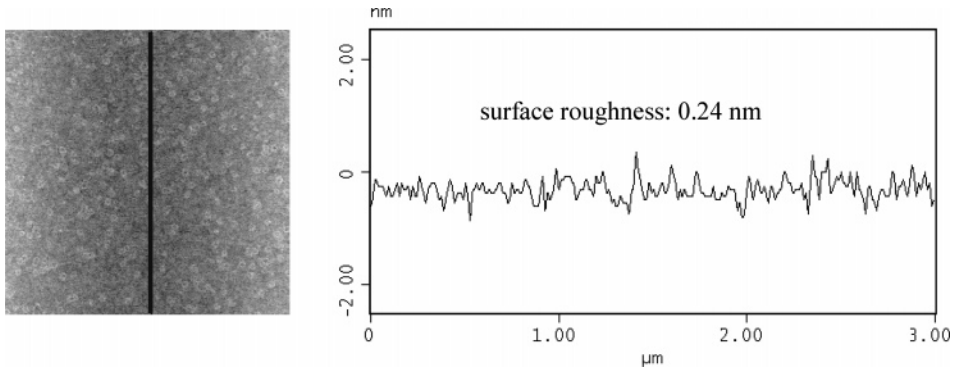

Figure 6. Section analysis of an AFM height image from the red phosphor sample after annealing at 1000 °C.

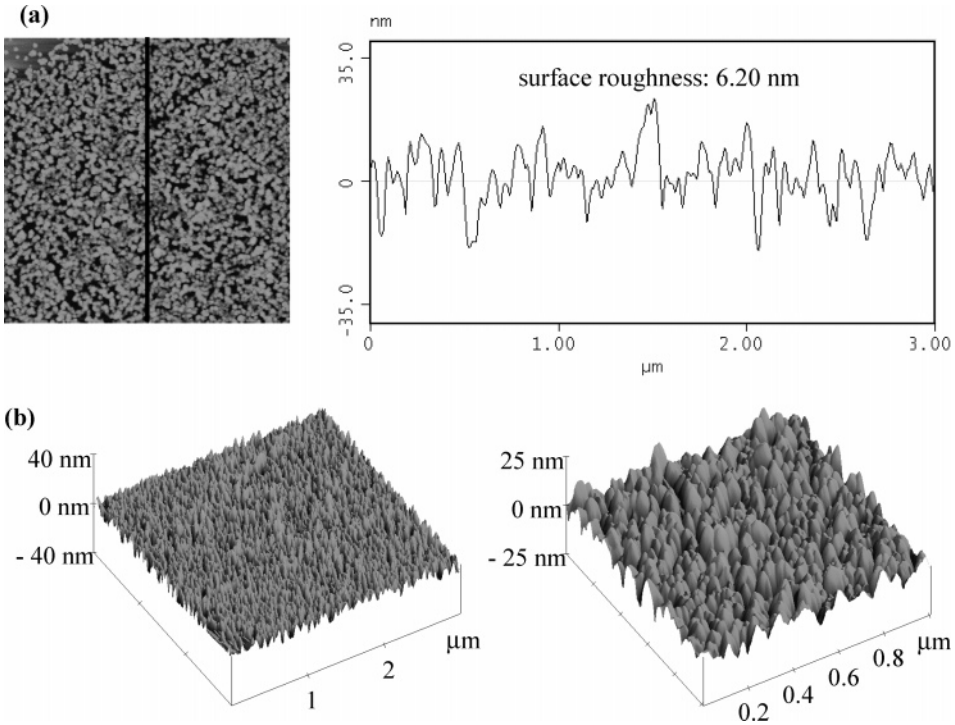

Figure 7. AFM height images from the green phosphor film after annealing at 1000 °C: (a) with section analysis of a 3 μm segment and (b) in side view in two different magnifications.

demanded active species after annealing at 1000 °C.

This reaction takes place under mass loss, because a part of the material is transferred to the gas phase. For the red phosphor material, the theoretical mass loss is rather low (27.4 wt %), but for the blue and the green phosphor samples the mass loss is notably larger (83.5 and 88.8 wt %, respectively) and is a basic problem for the formation of homogeneous thin films.

The inorganic films were analyzed through all stages (room temperature and after annealing at 200 and 1000 °C) with AFM. The resulting AFM amplitude pictures of the different "phosphor" films are shown in Figure 5.

The films of all three systems obtained at room temperature are very homogeneous, very flat, and typical for films prepared from either polymer or inorganic nanoparticles. After annealing the films at 200 °C, crystallization has taken place in all cases (as indicated by WAXS), and the domain growth is presumably due to Ostwald ripening. The flatness of all films prior to thermal decomposition is still very high.

Major differences arise after the solid-phase reaction at 1000 °C. The red phosphor sample with its low mass loss produces a very homogeneous thin film with an unusually low surface roughness of 0.24 nm, as quantified by surface roughness analysis (see Figure 6).

This value is as low as that of the silicone substrate (ca. 0.25 nm). We assume that the formed red phosphor film is essentially one large single crystal. We remind that already at room temperature, TEM (Figure 3b) indicated the formation of large platelets aligned parallel to the surface, which obviously support a very organized solid state transformation in a similarly ordered state. The thickness of the film can be analyzed in peripheral areas where holes down to the silicon support can be found. Here section analysis reveals a thickness of ca. 15 nm.

The calcined green phosphor film shows some surface textures (see Figure 7), but still a relatively homogeneous and thin film was created. Quantitative roughness analysis reveals a surface roughness of 6.2 nm (see Figure 7). This is quite amazing because of the high mass loss occurring throughout the calcination process. An explanation is given by the inside look shown in Figure 7b: the film obviously consists of monodisperse, densely packed, single nanoparticles. The particles have very likely evolved from the original miniemulsion

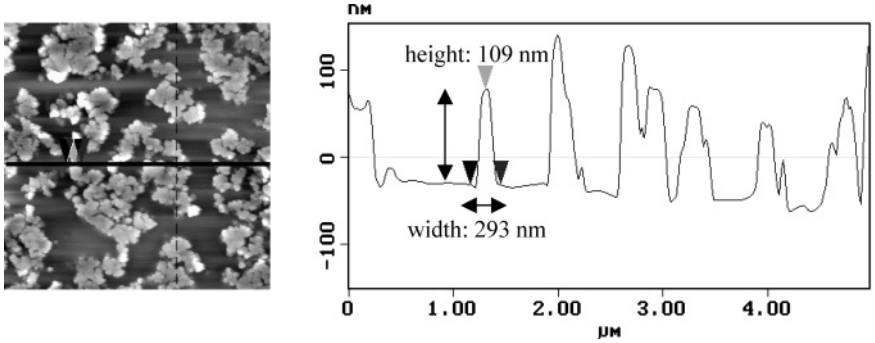

Figure 8. Section analysis of an AFM height image from the blue phosphor film after annealing at 1000 °C.

nanoparticles and show an average diameter of ca. 50−100 nm and a height of 25−30 nm.

The difference for the first two species is therefore mainly due to an altered nucleation rate and the resulting crystal habitus.

It was not possible to achieve the formation of a homogeneous thin film from the blue phosphor sample under the applied conditions. In this case, the combination of high mass loss during the solid phase reaction and improper crystal shape lead to noncohesive coatings. Figure 8 shows the typical morphology of well-separated blue phosphor dendrites with a height of ca. 100−150 nm (the height of the original miniemulsion monolayer) and diameters of several hundred nanometers. These terraces are presumably the product of a film rupture process due to mass loss, as the corresponding film at 200 °C is much better organized.

Conclusion and Outlook

It was shown that precursor nanoparticles of complex lanthanide phosphors with well-defined binary and ternary composition and high colloidal stability can be made by using the inverse miniemulsion process. The technique was applied to three systems that are chemically very different, ranging from slightly aqueous salt mixtures (red phosphor precursor) to highly acidic media (green phosphor) to rather highly aqueous solid/liquid nano-admixtures (blue phosphor). All precursor particles are mostly amorphous in dispersion, and can be used in a liquid coating process to obtain inorganic crystalline films which are very thin and highly homogeneous in their structures, as analyzed by AFM. In a subsequent annealing process, the precursor materials are converted to red, green, or blue phosphor films as they are used in television screens. In the case of red phosphor, "single crystal films" are formed which show a very low surface roughness, comparable to single crystal surfaces. The film quality obviously depends on crystal morphology and mass loss throughout solid-state transformation, as seen for the two other phosphors, for which system composition and calcination conditions still have to be optimized to end up with more useful crystalline inorganic films.

It is presumably the mostly amorphous character of the nanoparticles which enables in the first step homogeneous coating or film formation, very similar to the well-known case of polymer dispersion coatings. Standard wet-chemical or even mechanical procedures, on the other hand, do not allow the formation of inorganic films with a comparable structure, homogeneity, and thickness. In this context, the miniemulsion route toward structured inorganics possesses a high potential for subsequent industrial applications.

CM049958+